ADVANCED OPTICAL MATERIALS
www.advopticalmat.de

Efficient Sky-Blue Bipolar Delayed Fluorescence Luminogen for High-Performance Single Emissive Layer WOLEDs

Hao Chen, Huijun Liu, Pingchuan Shen, Jiajie Zeng, Ruming Jiang, Yan Fu, Zujin Zhao, and Ben Zhong Tang*

Luminogens with high photoluminescence efficiencies and high triplet (T_1) energy levels are desired to achieve high-performance white organic light-emitting diodes (WOLEDs). In this work, a sky-blue luminogen (DCB-BP-SFAC) with enhanced delayed fluorescence in aggregated state, bipolar carrier transport ability and high T_1 energy level is developed. DCB-BP-SFAC exhibits bright sky-blue electroluminescence (EL) in both non-doped and doped OLEDs with maximum external quantum efficiencies of 14.8% and 23.5%. DCB-BP-SFAC can function as efficient host for green, orange and red phosphorescent materials as well as thermally activated delayed fluorescence emitters with excellent EL performance. In addition, fluorescence/phosphorescence hybrid and all-fluorescence WOLEDs with a single emissive layer are fabricated by adopting DCB-BP-SFAC as emitter and host simultaneously. The all-fluorescence WOLED shows two-color warm-white light with good EL efficiencies of 47.1 cd A^{-1}, 46.2 lm W^{-1}, and 19.1%. The excellent performance of these OLEDs demonstrates the great application potential of DCB-BP-SFAC in practical display and lighting devices.

1. Introduction

Organic light-emitting diodes (OLEDs) have been regarded as a promising display technique owing to their prominent merits of self-luminescence, low cost, fast response, flexibility, and so forth.[1] In addition to monochromatic OLEDs, white OLEDs (WOLEDs) have also been developed rapidly in recent years as eye-protecting solid-state lighting sources.[2] To date, several innovative device architectures have been devised using various luminescent material systems to achieve high-performance WOLEDs.[3] Two-color and three-color multilayers WOLEDs with complex configurations are usually fabricated, in which, in most cases, one or more interlayers are required to balance carriers as well as confine excitons in different monochromatic layers.[4] To simplify device structure and production procedure as well as improve device stability, WOLEDs with a single emissive layer are considered as promising alternatives.[5] Appropriate robust materials that can function as both hosts and emitters are essential for single emissive layer WOLEDs, which should have good bipolar carrier transport ability, high triplet (T_1) energy level and, most importantly, excellent exciton utilization efficiency.

Conventional fluorescent materials can only harness 25% electrogenerated singlet excitons according to spin statistics.[6] Therefore, the utilization of the remaining 75% longer-lived triplet excitons has been regarded as the key to improve electroluminescence (EL) efficiencies of devices. Thermally activated delayed fluorescence (TADF) emitters are able to efficiently harvest both singlet and triplet excitons via reverse intersystem crossing (RISC) based on small energy splitting between lowest excited T_1 and lowest excited singlet state (S_1) (ΔE_{ST}).[7] And the small ΔE_{ST} can be realized by sufficiently separating the highest occupied molecular orbital (HOMO) and the lowest unoccupied molecular orbital (LUMO) via adopting highly twisted electron donor–acceptor (D–A) structures by molecular engineering.[8,9] Such kind of D–A structures are also conducive to achieving efficient bipolar carrier transport. In view of strong exciton harvest ability and bipolar carrier transport potential, TADF emitters are naturally ideal emitters and hosts for WOLEDs.

In this work, we wish to report the design and synthesis of a novel luminogen (DCB-BP-SFAC) with an asymmetric donor–acceptor–donor′ (D–A–D′) structure comprised of an acceptor of carbonyl group and two donors of 1,4-di(carbazol-9-yl)benzene (DCB) and spiro[acridine-9,9′-fluorene] (SFAC). The unsymmetrical structure may provide a higher possibility to modulate the optical property and carrier transport ability of the materials by introducing various functional groups at the same time. The carbonyl group is used as an electron acceptor

H. Chen, H. Liu, P. Shen, J. Zeng, R. Jiang, Y. Fu, Prof. Z. Zhao, Prof. B. Z. Tang
State Key Laboratory of Luminescent Materials and Devices
Guangdong Provincial Key Laboratory of Luminescence from Molecular Aggregates
SCUT-HKUST Joint Research Institute
South China University of Technology
Guangzhou 510640, China
E-mail: mszjzhao@scut.edu.cn
Prof. B. Z. Tang
Department of Chemistry
The Hong Kong University of Science & Technology
Clear Water Bay, Kowloon, Hong Kong 999077, China
Prof. B. Z. Tang
AIE Institute
Guangzhou Development District
Huangpu, Guangzhou 510530, China
The ORCID identification number(s) for the author(s) of this article can be found under https://doi.org/10.1002/adom.202002019.

DOI: 10.1002/adom.202002019

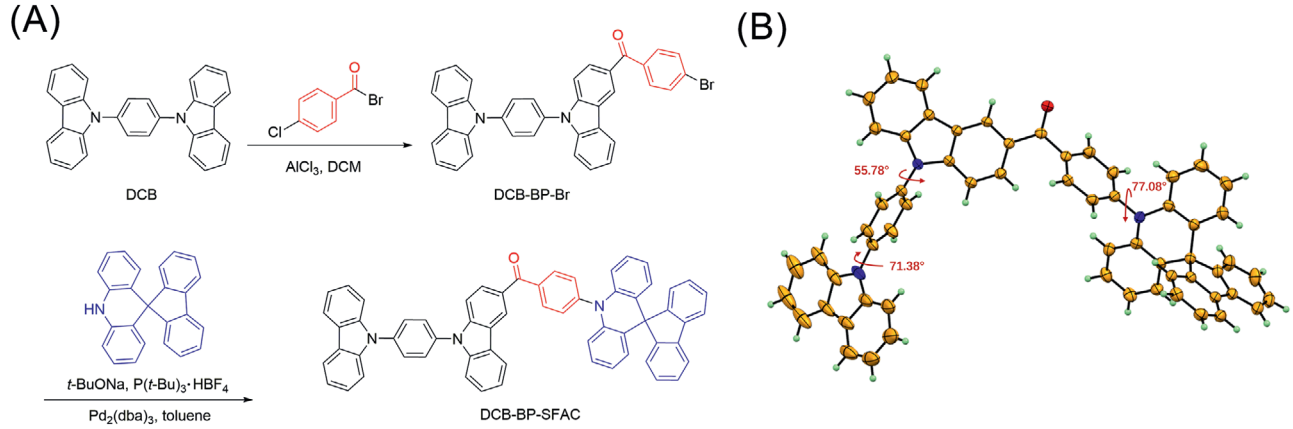

Figure 1. A) Synthetic route and B) crystal structure of DCB-BP-SFAC.

(A) because of not only its proper electron affinity but also the potential to facilitate intersystem crossing by increasing spin-orbit coupling.[10] The combination of carbonyl and SFAC groups is mainly responsible for creating a twisted D–A framework for the separation of HOMO and LUMO to achieve a small ΔE_{ST} for delayed fluorescence. The rigid and twisted structure with relatively weak electron-donating ability of SFAC is conducive to achieving efficient bluer emission. The DCB is capable of hole injection and transport as well as energy level modulation. The presence of DCB may also weaken the D–A interaction between carbonyl and SFAC groups, which is also favored for blue-shifted emission. The generated molecule DCB-BP-SFAC exhibits strong sky-blue delayed fluorescence in neat film and good bipolar transport ability. DCB-BP-SFAC can function not only as an efficient emitting layer to construct high-performance sky-blue non-doped/doped OLEDs but also as a robust host for green, orange and red phosphorescent materials as well as TADF emitters. Efficient two-color hybrid WOLEDs with a single emitting layer containing only a sky-blue host DCB-BP-SFAC and a red phosphorescent dopant $(Ir(piq)_2acac)$ are achieved. And more importantly, all-fluorescence WOLED with a single emitting layer of DCB-BP-SFAC doped with TADF dopant (TPA-AQ) are fabricated successfully, affording superior EL efficiencies of up to 47.1 cd A^{-1}, 46.2 lm W^{-1}, and 19.1%, indicating the device is among state-of-the-art all-fluorescence WOLEDs in the literature.

2. Result and Discussion

2.1. Synthesis and Characterization

The chemical structure and synthetic route of DCB-BP-SFAC is presented in **Figure 1**A. This molecule possesses a twisted D–A–D′ structure, which was constructed by two-step reactions of Friedel–Craft's acylation and subsequent Buchwald–Hartwig amination. The molecular structure was confirmed by ^1H and ^{13}C NMR and high-resolution mass spectrometry (HRMS), and the detailed synthetic procedures and characterization data are described in Supporting Information. DCB-BP-SFAC has good solubility in common organic solvents such as dichloromethane, chloroform, and tetrahydrofuran (THF), but is hardly soluble in water. DCB-BP-SFAC is highly thermal stable as evidenced by a very high decomposition temperature (T_d, corresponding to 5% weight loss) of 528 °C, examined by thermogravimetric analysis at a heating rate of 10 °C min^{-1} under nitrogen atmosphere (Figure S1, Supporting Information).

The single crystal of DCB-BP-SFAC was obtained in the mixture of dichloromethane/*n*-hexane at room temperature via slow solvent evaporation and the crystals structure is displayed in Figure 1B. It is found that DCB-BP-SFAC holds a highly twisted conformation, in which the SFAC moiety is connected to the adjacent phenylene substituent with a large torsion angle of 77.08°. And the DCB moiety is also highly twisted, with large torsion angles of 71.38 and 55.78° of the two carbazoles with central phenylene unit. This twisted conformation can well separate the HOMO and LUMO to lead a small ΔE_{ST}, and is also favored for effectively preventing close intermolecular π–π stacking to alleviate concentration quenching and exciton annihilation by Dexter energy transfer. Indeed, from the molecular packing mode of DCB-BP-SFAC in crystal (Figure S2, Supporting Information), DCB-BP-SFAC molecules are packed in a relatively loose manner without obvious π–π stacking interactions. While abundant C—H···π and C—H···O hydrogen bonds with distances of 2.436–2.733 Å are observed, which can enhance the stability and rigidify of the molecular structure and restrict intramolecular motion to alleviate nonradiative decay and thus enhance emission efficiency.

2.2. Frontier Orbital Distribution and Energy Levels

To investigate the geometrical and electronic structures of DCB-BP-SFAC, theoretical simulation is conducted by density functional theory and time-dependent density functional theory. The optimized molecular conformation and calculated frontier orbital distribution of DCB-BP-SFAC are displayed in **Figure 2**A. This molecule has a highly twisted structure with a separated distribution of the frontier orbitals. The HOMO is predominantly centered on electron-donating SFAC units, while the LUMO is mainly localized on electron-accepting carbonyl group and parts of adjacent aromatic rings. The efficient separation of HOMO and LUMO endows DCB-BP-SFAC with

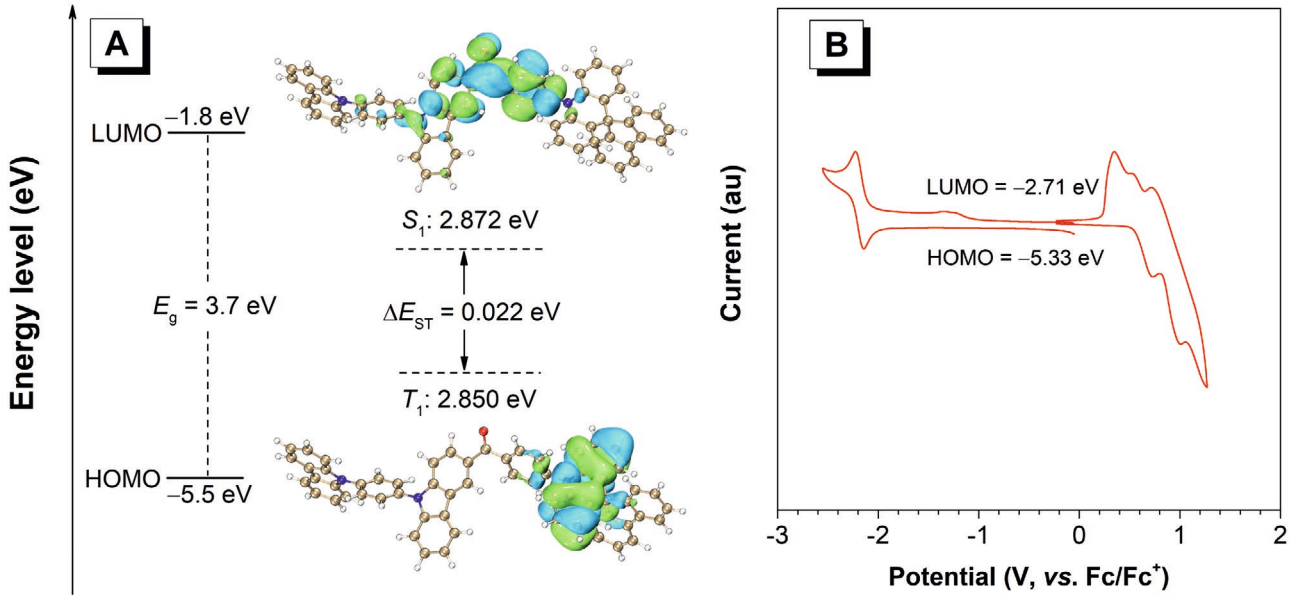

Figure 2. A) Calculated frontier orbital distribution and energy levels of DCB-BP-SFAC. B) Cyclic voltammogram of DCB-BP-SFAC, measured in dichloromethane (HOMO) and dimethylformamide (LUMO) containing 0.1 M tetrabutylammonium hexafluorophosphate. Scanning rate: 50 mV s^{-1}. The oxidation potential and reduction potentials are 0.53 and −2.09 V against the Fc/Fc^+ redox couple, corresponding to a HOMO level of −5.33 eV and LUMO level of −2.71 eV.

a small theoretical ΔE_{ST} of 0.022 eV, which is small enough to allow efficient RISC process from T_1 to S_1 states.

To determine practical HOMO and LUMO energy levels, cyclic voltammetry is carried out on the neat film of DCB-BP-SFAC. As illustrated in Figure 2B, DCB-BP-SFAC shows reversible oxidation and reduction processes, disclosing its good electrochemical stability. The HOMO and LUMO energy levels are calculated to be −5.33 and −2.71 eV, respectively, on the basis of the onsets of oxidation and reduction waves (HOMO = −[E_{ox} + 4.8] eV; LUMO = −[E_{re} + 4.8] eV, where E_{ox} and E_{re} represent the onset potentials of oxidation and reduction relative to Fc/Fc^+, respectively). Therefore, it is appropriate for carrier injection in OLEDs when DCB-BP-SFAC acts as emitter with NPB and TPBi as hole- and electron-transporting layers.

2.3. Photophysical Properties

DCB-BP-SFAC shows an absorption maximum at 338 nm in THF solution, which is generated by the π–π^* transition. Meanwhile, a weak and broad absorption tail extending to 420 nm is present (**Figure 3**A), which can be attributed to the intramolecular charge transfer (ICT) state between carbonyl group and SFAC moiety. It exhibits weak photoluminescence (PL) peaking at 510 nm in THF solution with a low PL quantum yield (Φ_{PL}) of 10.3%, while its vacuum-deposited neat film and doped film (40 wt% doping concentration with bis-(diphenylphosphoryl)-dibenzo[b,d]-furan-synonym (PPF) as host) radiates strong sky-blue PL at 482 and 478 nm with higher Φ_{PL} values of 70.8% and 92.2%, respectively, measured under nitrogen atmosphere.

The PL spectra of DCB-BP-SFAC in THF/water mixtures with different water fractions (f_w) are also recorded, where THF is the good solvent but water is the poor one for the molecule (Figure 3B). It can be found that the PL intensity decreases when water is added into THF solution and remains weak when the f_w is below 70 vol% due to the vigorous intramolecular motion as well as enhanced ICT effect.[11] The ICT effect can be verified by solvatochromism experiment in which the PL peak is red-shifted obviously as the increase of solvent polarity (Figure S3, Supporting Information). When the f_w is higher than 70 vol%, the PL intensity is increased greatly, owing to the aggregate formation, by which the intramolecular motion is greatly restricted, revealing that DCB-BP-SFAC has apparent aggregation-enhanced emission property.[12] Moreover, moderate blue-shifts are observed at high f_ws, which is attributed to the decreased polarity of the aggregate as well as rigidified molecular structure which can reduce reorganization energy of the excited state.

From the PL decay curves of DCB-BP-SFAC in THF and toluene solutions (10^{-5} M) under air or N_2 atmosphere (Figure S4, Supporting Information), it can be found that the PL lifetimes of DCB-BP-SFAC in these solutions are obviously increased in the absence of O_2, implying the existence of delayed fluorescence. On the other hand, the mean PL lifetime is greatly increased in neat film (3062.4 ns) relative to that in THF solution (165.5 ns), which is in good agreement with the prominent growing trend of PL lifetimes as the aggregate formation in THF/water mixtures (Figure 3C). The greatly enhanced delayed fluorescence with a longer lifetime of 7.9 µs and a higher ratio of delayed component of 38.4% in neat film relative to that in solution indicates the delayed fluorescence of DCB-BP-SFAC is enhanced by aggregate formation. In comparison with neat film, the doped film of DCB-BP-SFAC in PPF host has a slightly longer lifetime and a lower ratio of delayed fluorescence (**Table 1**).

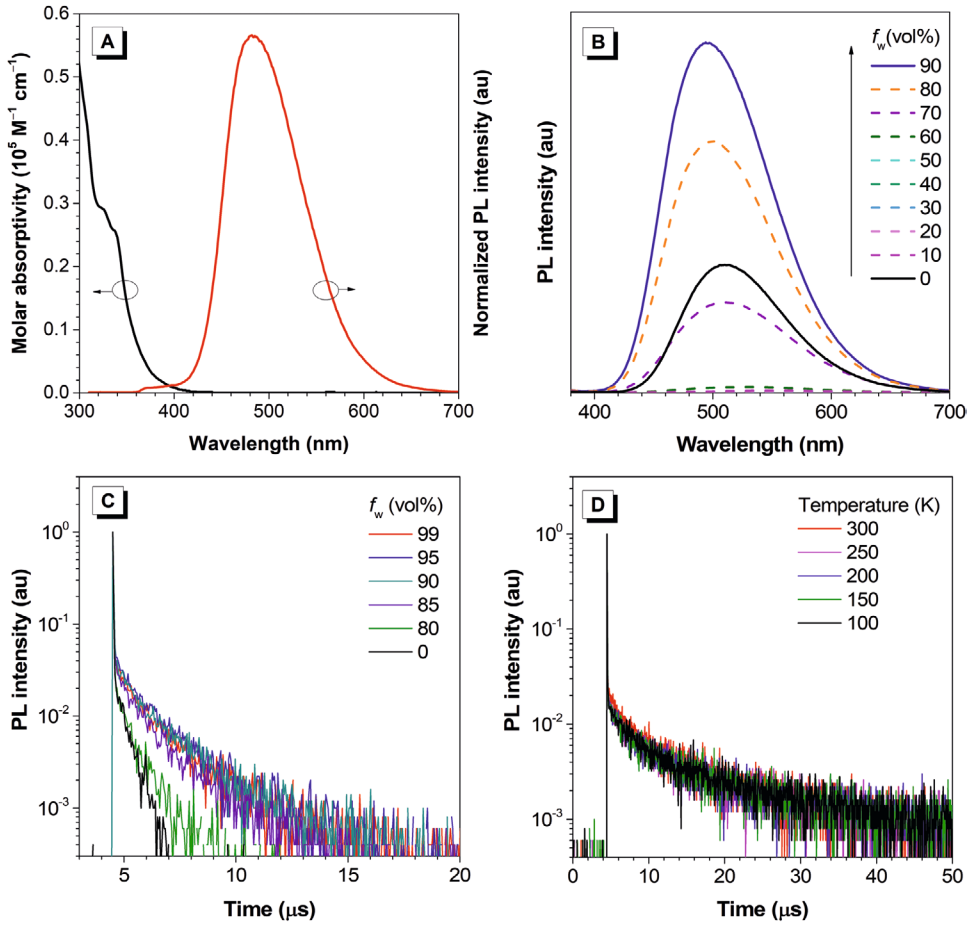

Figure 3. A) Absorption spectrum of DCB-BP-SFAC in THF solution (10^{-5} mol L^{-1}) and normalized PL spectrum of DCB-BP-SFAC in neat film. B) PL spectra and C) PL decay curves of DCB-BP-SFAC in THF/water mixtures with different water fractions (f_w) (10^{-5} M), measured under nitrogen. D) Temperature-dependent transient decay spectra of DCB-BP-SFAC in neat film, measured under nitrogen.

According to the temperature-dependent transient PL spectra (Figure 3D) of DCB-BP-SFAC in neat film under nitrogen atmosphere, it exhibits more prominent delayed fluorescence as the temperature increases from 100 to 300 K, demonstrating that DCB-BP-SFAC has a typical TADF character.[13] According to the fluorescence and phosphorescence spectra of the neat film recorded at 77 K (Figure S5, Supporting Information), DCB-BP-SFAC holds a high a small ΔE_{ST} of 0.025 eV, which is consistent with the theoretical value (0.022 eV). The doped film of DCB-BP-SFAC in PPF has a slightly larger ΔE_{ST} of 0.051 eV. These small ΔE_{ST} values can allow the fast RISC process, rendering efficient delayed fluorescence. Moreover, DCB-BP-SFAC also has a high T_1 energy level of 2.793 eV, which is higher than those of many traditional host materials, such as 4,4′-di(carbazol-9-yl)-1,1′-biphenyl (CBP) (2.6 eV).[14]

Table 1. The photophysical data of DCB-BP-SFAC.

	solution[a)]	neat film[b)]	doped film[b)]
λ_{abs} [nm]	338	338	324
λ_{em} [nm]	510	482	478
Φ_F[c)] [%]	10.3	70.8	92.2
$\langle\tau\rangle$[d)] [ns]	165.5	3062.4	3267.4
τ_{prompt}[e)] [ns]	16.4	25.8	22.9
$\tau_{delayed}$[e)] [μs]	0.5	7.9	9.5
$R_{delayed}$[f)] [%]	29.4	38.4	34.2
ΔE_{ST}[g)] [eV]	-	0.025	0.051

[a)]Measured in THF solution (10^{-5} M) at room temperature; [b)]Neat film and doped film (40 wt% doping concentration with PPF as host), vacuum-deposited on a quartz substrate; [c)]Determined by a calibrated integrating sphere under nitrogen at room temperature; [d)]Mean fluorescence lifetime evaluated at 300 K under nitrogen; [e)]Fluorescence lifetimes of prompt (τ_{prompt}) and delayed ($\tau_{delayed}$) components evaluated at 300 K under nitrogen; [f)]Ratio of delayed component; [g)]ΔE_{ST} = singlet–triplet energy splitting.

2.4. Sky-Blue OLEDs Based on DCB-BP-SFAC

Given the efficient sky-blue PL with prominent delayed fluorescence in neat film, the EL performance of DCB-BP-SFAC is investigated. The non-doped OLED (device B1) with a configuration of ITO/HATCN (5 nm)/NPB (30 nm)/mCP (10 nm)/DCB-BP-SFAC (20 nm)/PPF (10 nm)/TPBi (50 nm)/LiF (1 nm)/Al (120 nm) (**Figure 4**A) is fabricated by vacuum deposition technique, where the neat film of DCB-BP-SFAC functions

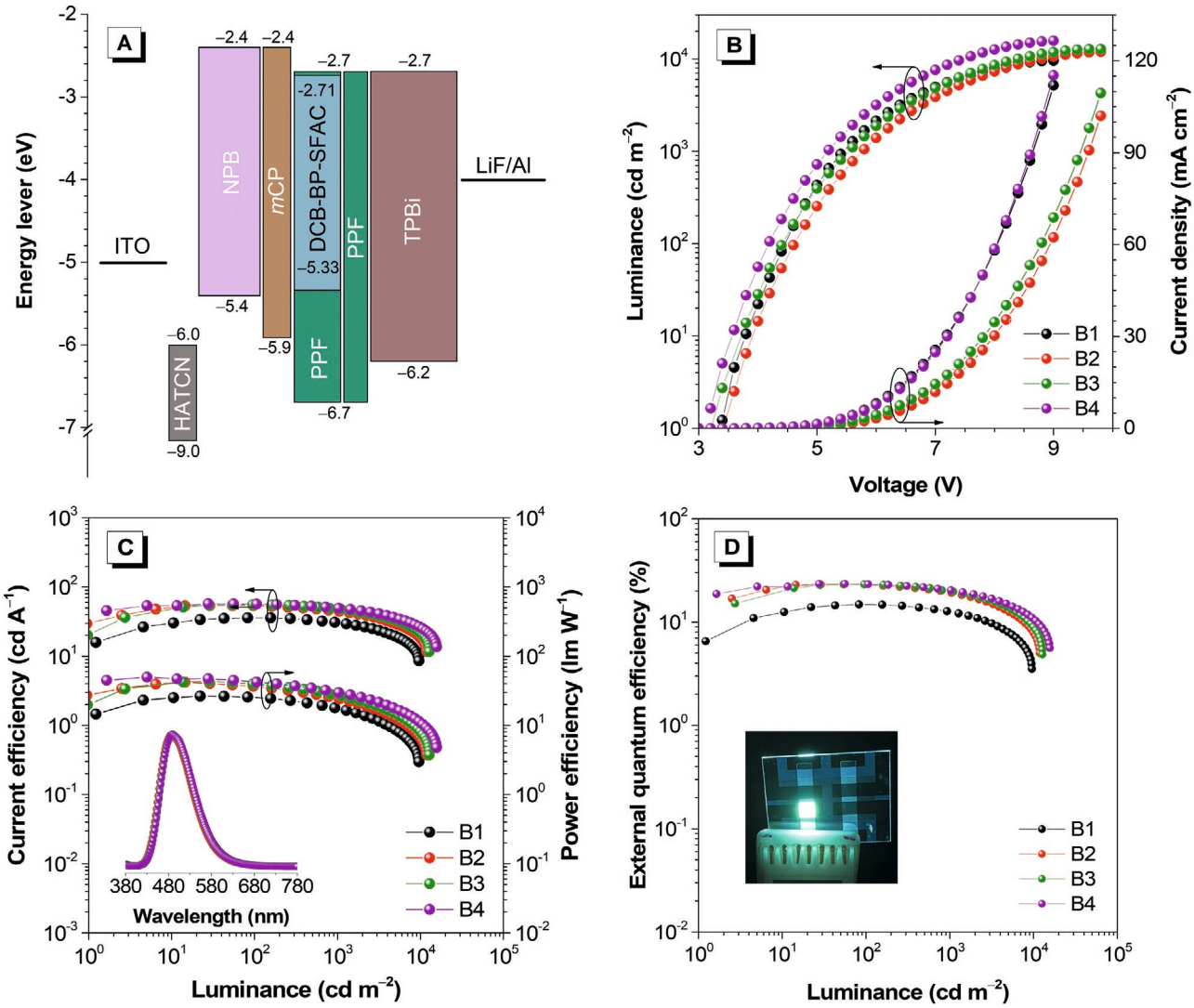

Figure 4. A) Device structures and energy diagrams. B) Luminance and current density curves with the change of voltage, and C) current efficiency and power efficiency curves with the change of luminance of devices B1–B4. Inset: EL spectra at 10 mA cm^{-2}. D) External quantum efficiency curves with the change of luminance. Inset: the photo of device B4 at 10 mA cm^{-2}.

as light-emitting layer, indium-tin oxide (ITO) is the transparent anode, 1,4,5,8,9,11-hexaazatriphenylene hexacarbonitrile (HATCN) works as hole injection layer, N,N′-bis(naphthalen-1-yl)-N,N′-bis(phenyl)benzidine (NPB) and 1,3,5-tris(N-phenylbenzimidazol-2-yl)benzene (TPBi) work as hole- and electron-transporting layers, respectively, and 9,9′-(1,3-phenylene)bis-9H-carbazole (mCP) and PPF function as electron- and hole-blocking layer, respectively. The device B1 can be turned on at a low voltage of 3.4 V and illuminates strong sky-blue light at 488 nm (CIE$_{x,y}$ = 0.198, 0.412), with peak luminance (L_{max}) of 9603 cd m^{-2} (**Table 2**). High EL efficiencies with peak values of current efficiency (η_C), power efficiency (η_P), and η_{ext} of 35.9 cd A^{-1}, 26.5 lm W^{-1} and 14.8%, respectively, are obtained in device B1. And at 1000 cd m^{-2}, this device still maintains good EL performance with η_C, η_P, and η_{ext} of 30.8 cd A^{-1}, 17.9 lm W^{-1}, and 12.7%, respectively. These excellent results are actually repeatable (Table S1, Supporting Information), indicating that DCB-BP-SFAC is a promising candidate for fabricating non-doped sky-blue OLEDs.

To further evaluate the potential application of DCB-BP-SFAC, doped OLEDs with a configuration of ITO/HATCN (5 nm)/NPB (30 nm)/mCP (10 nm)/*x* wt% DCB-BP-SFAC: PPF (20 nm)/PPF (10 nm)/TPBi (50 nm)/LiF (1 nm)/Al (120 nm) are fabricated. The emitting layers are comprised of DCB-BP-SFAC doped in PPF host with varied doping concentrations (x = 20, 30, and 40 for devices B2, B3, and B4, respectively). The obtained doped OLEDs also show excellent EL performances, with low turn-on voltages of 3.2–3.6 V and intense sky-blue light at 488 nm (Table 2). The device B4 owns the best EL efficiencies of 57.1 cd A^{-1}, 49.6 lm W^{-1}, and 23.5% (Figure 4B–D), and it still maintains excellent efficiencies of 49.5 cd A^{-1}, 29.9 lm W^{-1}, and 20.3% at 1000 cd m^{-2}, corresponding to a small efficiency roll-off of 13.6%, much superior to those of most TADF OLEDs with similar color (Table S2, Supporting Information).

Table 2. EL performance of sky-blue OLEDs.

Device[a)]	V_{on} [V]	L_{max} [cd m^{-2}]	η_C [cd A^{-1}]	η_P [lm W^{-1}]	η_{ext} [%]	λ_{EL} [nm]	CIE (x, y)
			maximum value/at 1000 cd m^{-2}				
B1	3.4	9603	35.9/30.8	26.5/17.9	14.8/12.7	488	(0.198,0.412)
B2	3.6	11918	53.8/44.5	41.9/24.1	23.1/19.1	488	(0.195,0.395)
B3	3.4	12792	55.7/47.4	43.1/26.6	23.1/19.7	488	(0.198,0.410)
B4	3.2	15724	57.2/49.5	49.6/29.9	23.5/20.3	488	(0.199,0.417)

[a)]Abbreviations: V_{on} = turn-on voltage at 1 cd m^{-2}; L_{max} = maximum luminance; $\eta_C/\eta_P/\eta_{ext}$ = current efficiency/power efficiency/external quantum efficiency; λ_{EL} = peaks of electroluminescence spectra at 10 mA cm^{-2}; CIE = Commission Internationale de l'Eclairage coordinates at 10 mA cm^{-2}.

2.5. Carrier Transport and Host Performance of DCB-BP-SFAC

To evaluate the potential of DCB-BP-SFAC as host, its carrier transport property is measured in hole- and electron-only devices with the structures of ITO/TAPC (10 nm)/DCB-BP-SFAC (80 nm)/TAPC (10 nm)/Al (120 nm) and ITO/TmPyPB (10 nm)/DCB-BP-SFAC (80 nm)/TmPyPB (10 nm)/LiF (1 nm)/Al (120 nm), respectively, via space charge limited current method.[15] The current density–voltage (J–V) relationship of electron- and hole-only devices are depicted in **Figure 5**A and the electric field-dependent mobilities (μ) of DCB-BP-SFAC is depicted in Figure 5B. For instance, at a practical electric field of 5.5×10^5 V cm^{-1}, the hole mobility (μ_h) and electron mobility (μ_e) of DCB-BP-SFAC are estimated to be 5.38×10^{-5} and 3.34×10^{-5} cm^2 V^{-1} s^{-1}, respectively, revealing the good bipolar carrier-transporting ability of DCB-BP-SFAC, which is beneficial to balance the holes and electrons in OLEDs and partially accounts for the excellent performances of non-doped and doped OLEDs with DCB-BP-SFAC as an emitter as well as a host. Thus, it is expected that such a bipolar luminogen with a high T_1 energy level (2.973 eV) and a high triplet exciton-harvesting efficiency can serve as efficient host for doped OLEDs based on phosphorescent materials and TADF emitters.

Three PhOLEDs with the device structures of ITO/HATCN (5 nm)/NPB (30 nm)/mCP (10 nm)/EML (20 nm)/PPF (10 nm)/TPBi (50 nm)/LiF (1 nm)/Al (120 nm) are fabricated to evaluate the potential of DCB-BP-SFAC as host, where the EML is the emitting layer composed by the DCB-BP-SFAC film doped with

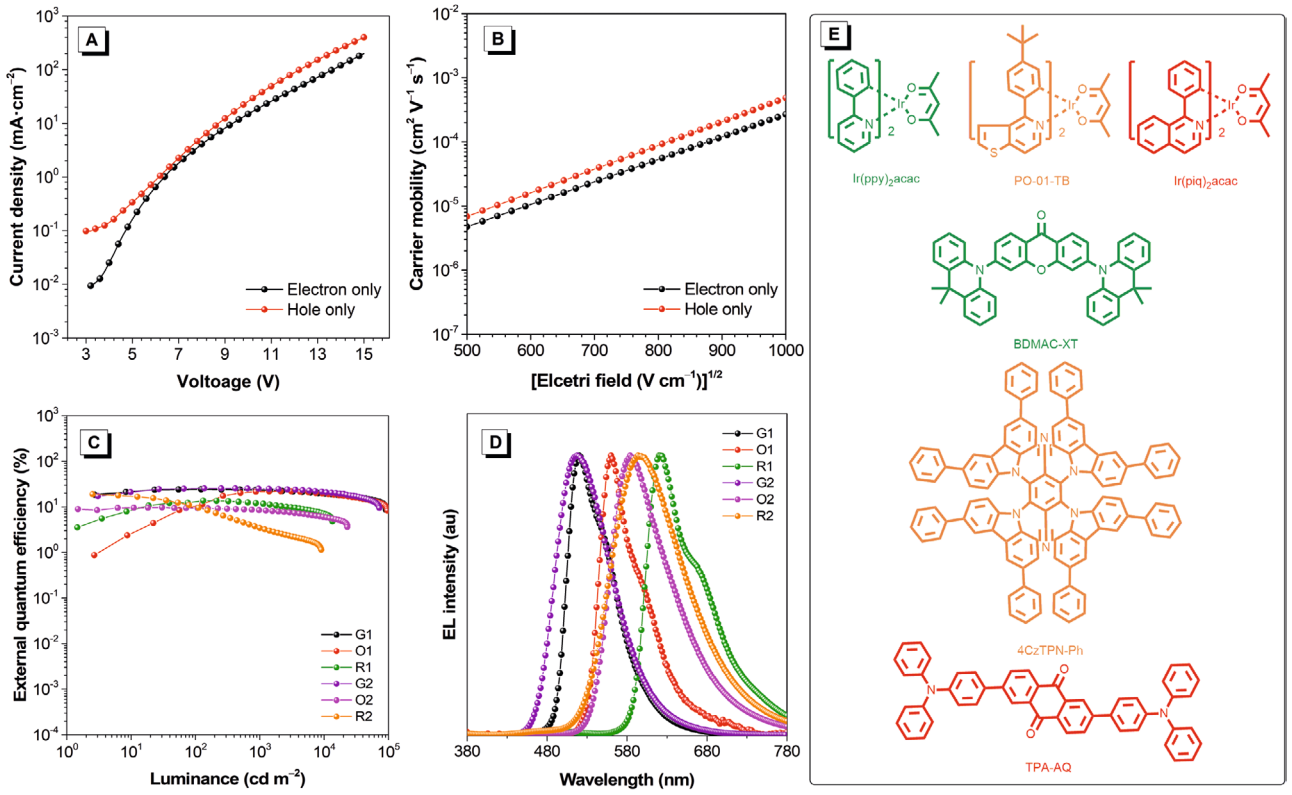

Figure 5. A) Current density curves with the change of voltage of the hole- and electron-only devices for DCB-BP-SFAC. B) Electric field-dependent carrier mobilities of DCB-BP-SFAC. C) External quantum efficiency curves with the change of luminance and D) EL spectra at 10 mA cm^{-2} of devices G1, O1, R1, G2, O2 and R3. E) Chemical structures of phosphorescent dopants and TADF emitters.

Table 3. EL performances of devices G1, O1, R1 G2, O2, and R2.

Device[a)]	V_{on} [V]	L_{max} [cd m^{-2}]	η_C [cd A^{-1}]	η_P [lm W^{-1}]	η_{ext} [%]	λ_{EL} [nm]	CIE (x, y)
			maximum value/at 1000 cd m^{-2}				
G1	3.0	91768	89.3/86.3	80.4/61.6	24.2/23.4	520	(0.298,0.637)
O1	3.2	96325	72.5/71.0	48.5/48.5	21.9/21.5	560	(0.475,0.519)
R1	3.2	13473	11.8/10.1	8.3/5.7	13.6/11.6	620	(0.658,0.326)
G2	3.2	72115	82.9/81.4	69.5/53.3	25.3/24.8	518	(0.275,0.587)
O2	3.6	22964	22.4/19.6	18.0/9.3	9.7/8.5	584	(0.545,0.451)
R2	3.0	13937	38.7/7.1	40.5/3.6	18.8/3.5	594	(0.544,0.445)

[a)]Abbreviations: V_{on} = turn-on voltage at 1 cd m^{-2}; L_{max} = maximum luminance; $\eta_C/\eta_P/\eta_{ext}$ = current efficiency/power efficiency/external quantum efficiency; λ_{EL} = peaks of electroluminescence spectra at 10 mA cm^{-2}; CIE = Commission Internationale de l'Eclairage coordinates at 10 mA cm^{-2}.

3 wt% phosphorescent dopants of green Ir(ppy)$_2$acac (device G1), orange PO-01-TB (device O1), or red Ir(piq)$_2$acac (device R1). The chemical structures of three phosphorescent dopants are shown in Figure 5E. These devices G1, O1, and R1 are turned on at low voltages of 3.0–3.2 V, and radiate very strong green, orange, and red light at 520, 560, and 620 nm, with maximum luminance of 91768, 96 325, and 13 478 cd m^{-2} and the peak external quantum efficiencies (η_{ext}s) of 24.2%, 21.9%, and 13.6%, respectively (**Table 3**). By surveying the EL spectra of PhOLEDs (Figure 5D), it can be found that the EL emission from DCB-BP-SFAC is totally absent at a high current density of 10 mA cm^{-2}, demonstrating that sufficient energy transfer from the host to the guest has been achieved at a doping concentration as low as 3 wt%. In view of the small efficiency roll-offs of both non-doped and doped OLEDs using DCB-BP-SFAC as emitter, the annihilation of triplet excitons on DCB-BP-SFAC should have been suppressed greatly. Therefore, in PhOLEDs using DCB-BP-SFAC as host, most excitons formed on DCB-BP-SFAC are transferred to phosphorescent dopants to achieve excellent EL efficiencies and small efficiency roll-off as well.

In addition to serve as host for phosphorescent materials, DCB-BP-SFAC can also be used as host for TADF emitters. Herein, we choose green, orange, and red TADF emitters of 3,6-bis(9,9-dimethylacridin-10-yl)-xanthen-9-one (BDMAC-XZ),[16] 2,3,5,6-tetrakis(3,6-diphenyl-carbazol-9-yl)terephthalonitrile (4CzTPN-Ph)[17] and 2,6-bis(4-(diphenylamino)phenyl) anthracene-9,10-dione (TPA-AQ),[18] respectively (Figure 5E), which were reported to have the η_{ext} of 25%, 11.2%, and 12.5%, in doped OLEDs with CBP as host. With the same device structures as those of above doped PhOLEDs, devices G2, O2, and R2 are fabricated by adopting a green-emitting layer of DCB-BP-SFAC doped with 30 wt% BDMAC-XT, an orange-emitting layer of DCB-BP-SFAC doped with 5 wt% 4CzTPN-Ph and a red-emitting layer of DCB-BP-SFAC doped with 3 wt% TPA-AQ, respectively. Delightfully, devices G2, O2, and R2 exhibit impressive EL performance with peak η_{ext} values of 25.3%, 9.7%, and 18.8%, respectively (Figure 5C). The EL efficiencies of devices G2 and O2 are comparable to the reported values, while the performances of device R2 are much better than those of TPA-AQ in CBP host (Table S3, Supporting Information), disclosing that DCB-BP-SFAC is a capable host for not only phosphorescent materials but also TADF emitters, particularly red TADF emitters.

2.6. Single Emissive Layer WOLEDs

Encouraged by the superior performances of DCB-BP-SFAC as emitter and host, we look forward to its application in single emissive layer WOLEDs. Herein, it is utilized as both host and emitter to prepare two-color WOLEDs (device W1) based on a hybrid single emissive layer with a configuration of ITO/HATCN (5 nm)/NPB (30 nm)/mCP (10 nm)/0.3 wt% Ir(piq)$_2$acac: DCB-BP-SFAC (20 nm)/PPF (10 nm)/TPBi (50 nm)/LiF (1 nm)/Al (120 nm). For single emissive layer WOLEDs, the energy transfer should be well regulated by delicately adjusting the doping concentrations to realize white light emission with high efficiency. In the EML of 0.3 wt% Ir(piq)$_2$acac: DCB-BP-SFAC in device W1, the host DCB-BP-SFAC can harvest both singlet and triplet excitons via RISC from T_1 to S_1 for radiative decay directly to supply sky-blue light as well as to excite phosphorescent guest Ir(piq)$_2$acac through efficient energy transfer process to acquire red light concurrently. The presence of complementary colors of red and sky-blue leads to white light with a Commission Internationale de l'Eclairage (CIE) coordinates of (0.333, 0.397) and a high Color Rendering Index (CRI) of 77.3 at 1000 cd m^{-2}. Moreover, excellent EL performance with peak η_C, η_P, and η_{ext} of 31.2 cd A^{-1}, 28.3 lm W^{-1}, and 17.8%, respectively, have been attained in device W1 (**Table 4**).

Due to the high price of phosphorescent materials containing noble metals, purely organic luminescent materials with fluorescence or delayed fluorescence (all-fluorescence) could be ideal alternatives, but the performances of reported all-fluorescence WOLEDs are still unsatisfactory. Here, all-fluorescence WOLEDs are fabricated with a configuration of ITO/HATCN (5 nm)/NPB (30 nm)/mCP (10 nm)/0.5 wt% TPA-AQ: DCB-BP-SFAC (20 nm)/PPF (10 nm)/TPBi (50 nm)/LiF (1 nm)/Al (120 nm) (device W2), in which the TADF emitter TPA-AQ functions as red dopant and DCB-BP-SFAC works as host and sky-blue emitter. In device W2, most excitons are formed on DCB-BP-SFAC due to the low dopant concentration, and a part of excitons can decay immediately to generate sky-blue light, while the others migrate to the red TADF dopant to provide red light. It is inspiring that device W2 shows superior EL performance with peak η_C, η_P, and η_{ext} of 47.1 cd A^{-1}, 46.2 lm W^{-1}, and 19.1%, respectively, which are much better than those obtained in device W1. By comparing

Table 4. EL performance of WOLEDs.

Device[a)]	V_{on} [V]	L_{max} [cd m^{-2}]	η_C [cd A^{-1}]	η_P [lm W^{-1}]	η_{ext} [%]	CIE (x, y)	CRI
			maximum value/at 1000 cd m^{-2}				
W1	3.2	8479	31.2/19.4	28.3/10.9	17.8/10.1	(0.333, 0.397)	77.3
W2	3.2	11750	47.1/17.8	46.2/10.0	19.1/7.4	(0.476, 0.458)	56.7

[a)]Abbreviations: V_{on} = turn-on voltage at 1 cd m^{-2}; L_{max} = maximum luminance; $\eta_C/\eta_P/\eta_{ext}$ = current efficiency/power efficiency/external quantum efficiency; CIE = Commission Internationale de l'Eclairage coordinates at 1000 cd m^{-2}. CRI = Color Rendering Index coordinates at 1000 cd cm^{-2}.

the EL spectra of devices W1 and W2, it can be seen that the red light peak of device W2 is much stronger than that of device W1, while the sky-blue light peak of device W1 is much weaker (**Figure 6**). This leads to warm-white light with CIE$_{x,y}$ coordinates of (0.476, 0.458) of W2 at 1000 cd m^{-2}, which is of high potential as a healthy lighting source. The CRI value of W2 is 56.7, which can be increased by enhancing the concentration of TPA-AQ (Table S4, Supporting Information). These results demonstrate that all-fluorescence WOLEDs with a single emissive layer composed of DCB-BP-SFAC and TPA-AQ can afford warm-white light and excellent EL performance. To the best of knowledge, device W2 is among state-of-the-art all-fluorescence single emissive layer WOLEDs ever reported (Table S5, Supporting Information).[19]

3. Conclusion

In conclusion, a new sky-blue luminogen DCB-BP-SFAC is designed and synthesized, with a carbonyl acceptor and DCB and SFAC donors. DCB-BP-SFAC holds good thermal and electrochemical stabilities, and shows evidently enhanced delayed fluorescence in the aggregated state. Non-doped and doped sky-blue OLEDs are obtained by using DCB-BP-SFAC as emitter, providing excellent EL performance with excellent η_{ext} values of up to 23.5% and small roll-off. Owing to its high exciton harness efficiency, good bipolar carrier transport ability and high T_1 energy level, DCB-BP-SFAC can serve as host for efficient green, orange, and red PhOLEDs with high η_{ext} values of 24.2%, 21.9%, and 13.6%, respectively, and for green and orange

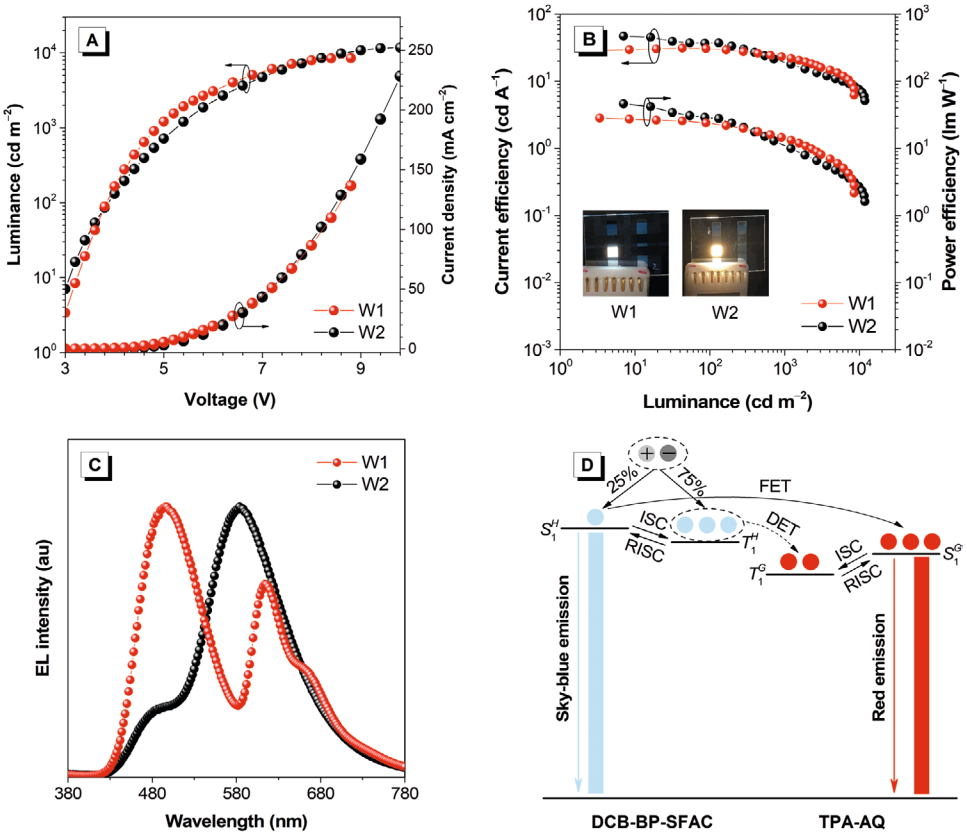

Figure 6. A) Luminance and current density curves with the change of voltage of devices W1 and W2. B) Current efficiency and power efficiency curves with the change of luminance of devices W1 and W2. C) EL spectra of devices W1 and W2 at 1000 cd m^{-2}. D) Diagram of energy transfer and emission processes in device W2.

TADF OLED with high η_{ext} values of 25.3% and 9.7%, and more importantly for red TADF OLED of TPA-AQ, with an enhanced η_{ext} value of 18.3%. Meanwhile, single emissive layer fluorescence/phosphorescence hybrid WOLEDs utilizing DCB-BP-SFAC as emitter and host simultaneously realize a high CRI of 77.3 and EL efficiencies of 31.2 cd A^{-1}, 28.3 lm W^{-1}, and 17.8%. Furthermore, high-performance all-fluorescence warm-white OLEDs with a single emissive layer are also obtained based on DCB-BP-SFAC and TADF dopant TPA-AQ, giving impressive peak η_C, η_P, and η_{ext} of 47.1 cd A^{-1}, 46.2 lm W^{-1}, and 19.1%, respectively. All above outstanding performances of OLEDs based on DCB-BP-SFAC as emitter or host undoubtedly demonstrate its practicable multifunctionality and great application potential in displays and lightings.

4. Experimental Section

(4-(Spiro[acridine-9,9′-fluoren]-10-yl)phenyl)(9-(4-(9H-carbazol-yl)phenyl)-carbazol-3-yl)methanone (DCB-BP-SFAC): A mixture of DCB-BP-Br (1.1 mmol, 0.649 g), *t*-BuONa (2.2 mmol, 211 mg), P(*t*-Bu)$_3$·HBF$_4$ (0.88 mmol, 26 mg), Pd$_2$(dba)$_3$ (0.22 mmol, 20 mg), and 10H-spiro[acridine-9,9′-fluorene] (1.32 mmol, 0.437 g) was added to a two-neck flask, evacuated, and backfilled with dry nitrogen. After that, 80 mL toluene was added into the flask. The reaction mixture was refluxed at 110 °C for 12 h and then cooled down to room temperature. The mixture was poured into water and extracted with dichloromethane (20 mL) for three times. The combined organic layers were washed with water and dried over anhydrous Na_2SO_4. After filtration and solvent evaporation under reduced pressure, the residue was purified via silica-gel column chromatography using dichloromethane/petroleum as eluent. DCB-BP-SFAC was obtained as sky-blue solid in 91.8% yield. ^{1}H NMR (500 MHz, $CDCl_3$) δ 8.86 (d, J = 1.4 Hz, 1H), 8.29 (d, J = 7.7 Hz, 1H), 8.26–8.19 (m, 4H), 8.16–8.13 (m, 1H), 7.93–7.85 (m, 4H), 7.82 (d, J = 7.6 Hz, 2H), 7.71–7.66 (m, 3H), 7.63–7.53 (m, 4H), 7.52–7.47 (m, 2H), 7.47–7.34 (m, 7H), 7.29–7.27 (m, 2H), 7.01–6.97 (m, 2H), 6.65–6.59 (m, 2H), 6.48–6.44 (m, 4H); ^{13}C NMR (125 MHz, $CDCl_3$) δ 195.59, 156.45, 144.57, 143.50, 141.72, 140.93, 140.64, 139.25, 138.76, 137.53, 135.72, 132.80, 131.36, 129.54, 128.97, 128.55, 128.51, 128.40, 127.96, 127.65, 127.30, 127.13, 126.19, 125.76, 125.02, 123.91, 123.67, 123.56, 123.46, 121.38, 120.94, 120.53, 120.44, 119.94, 114.60, 110.34, 109.69, 109.59, 77.26, 77.22, 77.01, 76.75, 56.78, 0.00; HRMS (MALDI-TOF): m/z [M$^+$] calcd. $C_{62}H_{39}N_3O$, 841.3093; found, 841.3089.

Crystal Data of DCB-BP-SFAC: (CCDC 2044250): $C_{62}H_{39}N_3O$, M_W = 841.96, orthorhombic, Pbca, a = 7.8032(2), b = 30.1972(6), c = 43.2659(7) Å, α = 89.9999(15)°, β = 90.0175(18)°, γ = 90.0096(19)°, V = 10194.9(4) Å^3, Z = 8, Dc = 1.097 g cm^{-3}, μ = 0.504 mm^{-1} (CuKα, λ = 1.54184), F(000) = 3520, T = 149.99(10) K, $2\theta_{max}$ = 67.074° (98.90%), 32934 measured reflections, 9006 independent reflections (R_{int} = 0.0508), GOF on F^2 = 0.997, R_1 = 0.0709, wR_2 = 0.1295 (all data), Δe 0.151 and –0.200 eÅ^{-3}.

Supporting Information

Supporting Information is available from the Wiley Online Library or from the author.

Acknowledgements

This work was financially supported by the National Natural Science Foundation of China (21788102), the Natural Science Foundation of Guangdong Province (2019B030301003), and the Fundamental Research Funds for the Central Universities.

Conflict of Interest

The authors declare no conflict of interest.

Data Availability Statement

Research data are not shared.

Keywords

aggregation-enhanced emission, bipolar carrier transport, host materials, organic light-emitting diodes, thermally activated delayed fluorescence

Received: November 23, 2020
Revised: January 30, 2021
Published online: March 1, 2021

[1] a) H. Sasabe, J. Kido, *J. Mater. Chem. C* **2013**, *1*, 1699; b) B. Chen, B. Liu, J. Zeng, H. Nie, Y. Xiong, J. Zou, H. Ning, Z. Wang, Z. Zhao, B. Z. Tang, *Adv. Funct. Mater.* **2018**, *28*, 1803369; c) X. Y. Cai, S. J. Su, *Adv. Funct. Mater.* **2018**, *28*, 1802558; d) T. Ohsawa, H. Sasabe, T. Watanabe, K. Nakao, R. Komatsu, Y. Hayashi, Y. Hayasaka, J. Kido, *Adv. Opt. Mater.* **2019**, *7*, 1801282; e) J. Yang, L. Li, Y. Yu, Z. Ren, Q. Peng, S. Ye, Q. Li, Z. Li, *Mater. Chem. Front.* **2017**, *1*, 91.

[2] a) B. W. D'Andrade, S. R. Forrest, *Adv. Mater.* **2004**, *16*, 1585; b) D. D. Zhang, P. C. Wei, D. Q. Zhang, L. Duan, *ACS Appl. Mater. Interfaces* **2017**, *9*, 19040; c) F. Zhao, D. Ma, *Mater. Chem. Front.* **2017**, *1*, 1933; d) Z. Wang, X.-L. Li, Z. Ma, X. Cai, C. Cai, S.-J. Su, *Adv. Funct. Mater.* **2018**, *28*, 1706922; e) X. Tang, X. Y. Liu, Z. Q. Jiang, L. S. Liao, *Adv. Funct. Mater.* **2019**, *29*, 1807541; f) Q. Liang, C. Han, C. Duan, H. Xu, *Adv. Opt. Mater.* **2018**, *6*, 1800020; g) X. K. Liu, Z. Chen, J. Qing, W. J. Zhang, B. Wu, H. L. Tam, F. Zhu, X. H. Zhang, C. S. Lee, *Adv. Mater.* **2015**, *27*, 7079; h) J. Liang, C. Li, X. Zhuang, K. Ye, Y. Liu, Y. Wang, *Adv. Funct. Mater.* **2018**, *28*, 1707002.

[3] a) J. Kido, H. Shionoya, K. Nagai, *Appl. Phys. Lett.* **1995**, *67*, 2281; b) Y. Sun, N. C. Giebink, H. Kanno, B. Ma, M. E. Thompson, S. R. Forrest, *Nature* **2006**, *440*, 908; c) S. Reineke, F. Lindner, G. Schwartz, N. Seidler, K. Walzer, B. Lussem, K. Leo, *Nature* **2009**, *459*, 234.

[4] a) B. Liu, H. Nie, X. Zhou, S. Hu, D. Luo, D. Gao, J. Zou, M. Xu, L. Wang, Z. Zhao, A. Qin, J. Peng, H. Ning, Y. Cao, B. Z. Tang, *Adv. Funct. Mater.* **2016**, *26*, 776; b) Z. Wu, L. Yu, F. Zhao, X. Qiao, J. Chen, F. Ni, C. Yang, T. Ahamad, S. M. Alshehri, D. Ma, *Adv. Opt. Mater.* **2017**, *5*, 1700415; c) X. Chen, Z. Yang, W. Li, Z. Mao, J. Zhao, Y. Zhang, Y. C. Wu, S. Jiao, Y. Liu, Z. Chi, *ACS Appl. Mater. Interfaces* **2019**, *11*, 39026.

[5] a) X.-K. Liu, C.-J. Zheng, M.-F. Lo, J. Xiao, Z. Chen, C.-L. Liu, C.-S. Lee, M.-K. Fung, X.-H. Zhang, *Chem. Mater.* **2013**, *25*, 4454; b) B. Liu, L. Wang, D. Gao, M. Xu, X. Zhu, J. Zou, L. Lan, H. Ning, J. Peng, Y. Cao, *Mater. Horiz.* **2015**, *2*, 536; c) C. Cao, W. C. Chen, J. X. Chen, L. Yang, X. Z. Wang, H. Yang, B. Huang, Z. L. Zhu, Q. X. Tong, C. S. Lee, *ACS Appl. Mater. Interfaces* **2019**, *11*, 11691; d) Y. Miao, K. Wang, B. Zhao, L. Gao, Y. Wang, H. Wang, B. Xu, F. Zhu, *J. Mater. Chem. C* **2017**, *5*, 12474.

[6] a) D. Y. Kondakov, *J. Soc. Inf. Disp.* **2009**, *17*, 2; b) M. Pope, H. P. Kallmann, P. Magnante, *J. Chem. Phys.* **1963**, *38*, 2042; c) X. Song, D. Zhang, Y. Lu, C. Yin, L. Duan, *Adv. Mater.* **2019**, *31*, 1901923; d) K. H. Lee, J. Y. Lee, *Adv. Opt. Mater.* **2020**, *8*, 2000328;

e) S. Gan, W. Luo, B. He, L. Chen, H. Nie, R. Hu, A. Qin, Z. Zhao, B. Z. Tang, *J. Mater. Chem. C* **2016**, *4*, 3705.

[7] a) K. Goushi, K. Yoshida, K. Sato, C. Adachi, *Nat. Photonics* **2012**, *6*, 253; b) S. Hirata, Y. Sakai, K. Masui, H. Tanaka, S. Y. Lee, H. Nomura, N. Nakamura, M. Yasumatsu, H. Nakanotani, Q. Zhang, K. Shizu, H. Miyazaki, C. Adachi, *Nat. Mater.* **2015**, *14*, 330; c) Z. Yang, Z. Mao, Z. Xie, Y. Zhang, S. Liu, J. Zhao, J. Xu, Z. Chi, M. P. Aldred, *Chem. Soc. Rev.* **2017**, *46*, 915; d) Y. Yuan, Y. Hu, Y.-X. Zhang, J.-D. Lin, Y.-K. Wang, Z.-Q. Jiang, L.-S. Liao, S.-T. Lee, *Adv. Funct. Mater.* **2017**, *27*, 1700986; e) T. Yang, Z. Cheng, Z. Li, J. Liang, Y. Xu, C. Li, Y. Wang, *Adv. Funct. Mater.* **2020**, *30*, 2002681.

[8] a) Q. Zhang, B. Li, S. Huang, H. Nomura, H. Tanaka, C. Adachi, *Nat. Photonics* **2014**, *8*, 326; b) D. Zhang, M. Cai, Z. Bin, Y. Zhang, D. Zhang, L. Duan, *Chem. Sci.* **2016**, *7*, 3355; c) Y. Yuan, X. Tang, X. Y. Du, Y. Hu, Y. J. Yu, Z. Q. Jiang, L. S. Liao, S. T. Lee, *Adv. Opt. Mater.* **2019**, *7*, 1801536; d) I. S. Park, H. Komiyama, T. Yasuda, *Chem. Sci.* **2017**, *8*, 953; e) D. H. Ahn, H. Lee, S. W. Kim, D. Karthik, J. Lee, H. Jeong, J. Y. Lee, J. H. Kwon, *ACS Appl. Mater. Interfaces* **2019**, *11*, 14909.

[9] a) J. Guo, Z. Zhao, B. Z. Tang, *Adv. Opt. Mater.* **2018**, *6*, 1800264; b) J. Huang, H. Nie, J. Zeng, Z. Zhuang, S. Gan, Y. Cai, J. Guo, S.-J. Su, Z. Zhao, B. Z. Tang, *Angew. Chem., Int. Ed.* **2017**, *56*, 12971; c) B. S. Kim, J. Y. Lee, *Adv. Funct. Mater.* **2014**, *24*, 3970; d) H. Kaji, H. Suzuki, T. Fukushima, K. Shizu, K. Suzuki, S. Kubo, T. Komino, H. Oiwa, F. Suzuki, A. Wakamiya, Y. Murata, C. Adachi, *Nat. Commun.* **2015**, *6*, 8476.

[10] a) J. Guo, X.-L. Li, H. Nie, W. Luo, S. Gan, S. Hu, R. Hu, A. Qin, Z. Zhao, S.-J. Su, B. Z. Tang, *Adv. Funct. Mater.* **2017**, *27*, 1606458; b) H. Liu, J. Zeng, J. Guo, H. Nie, Z. Zhao, B. Z. Tang, *Angew. Chem., Int. Ed.* **2018**, *57*, 9290; c) J. Zeng, J. Guo, H. Liu, J. W. Y. Lam, Z. Zhao, S. Chen, B. Z. Tang, *Chem. - Asian J.* **2019**, *14*, 828; d) J. Huang, Z. Xu, Z. Cai, J. Guo, J. Guo, P. Shen, Z. Wang, Z. Zhao, D. Ma, B. Z. Tang, *J. Mater. Chem. C* **2019**, *7*, 330; e) Y. Fu, H. Liu, X. Zhu, J. Zeng, Z. Zhao, B. Z. Tang, *J. Mater. Chem. C* **2020**, *8*, 9549.

[11] a) W. Qin, D. Ding, J. Liu, W. Z. Yuan, Y. Hu, B. Liu, B. Z. Tang, *Adv. Funct. Mater.* **2012**, *22*, 771; b) Y. Huang, J. Mei, X. Ma, *Dyes Pigm.* **2019**, *165*, 499; c) J. Yang, Y. Gao, T. Jiang, W. Liu, C. Liu, N. Lu, B. Li, J. Mei, Q. Peng, J. Hua, *Mater. Chem. Front.* **2017**, *1*, 1396.

[12] a) Z. Zhao, J. W. Y. Lam, C. Y. Chan, S. Chen, J. Liu, P. Lu, M. Rodriguez, J. L. Maldonado, G. Ramos-Ortiz, H. H. Sung, I. D. Williams, H. Su, K. S. Wong, Y. Ma, H. S. Kwok, H. Qiu, B. Z. Tang, *Adv. Mater.* **2011**, *23*, 5430; b) W. Luo, H. Nie, B. He, Z. Zhao, Q. Peng, B. Z. Tang, *Chem. - Eur. J.* **2017**, *23*, 18041; c) B. Chen, Y. Jiang, L. Chen, H. Nie, B. He, P. Lu, H. H. Y. Sung, I. D. Williams, H. S. Kwok, A. Qin, Z. Zhao, B. Z. Tang, *Chem. - Eur. J.* **2014**, *20*, 1931; d) J. Zeng, J. Guo, H. Liu, Z. Zhao, B. Z. Tang, *Adv. Funct. Mater.* **2020**, *30*, 2000019.

[13] a) L. Zhan, Z. Chen, S. Gong, Y. Xiang, F. Ni, X. Zeng, G. Xie, C. Yang, *Angew. Chem., Int. Ed.* **2019**, *58*, 17651; b) P. L. Dos Santos, J. S. Ward, M. R. Bryce, A. P. Monkman, *J. Phys. Chem. Lett.* **2016**, *7*, 3341; c) G. Meng, X. Chen, X. Wang, N. Wang, T. Peng, S. Wang, *Adv. Opt. Mater.* **2019**, *7*, 1900130; d) V. Jankus, P. Data, D. Graves, C. McGuinness, J. Santos, M. R. Bryce, F. B. Dias, A. P. Monkman, *Adv. Funct. Mater.* **2014**, *24*, 6178.

[14] a) M. A. Baldo, S. R. Forrest, *Phys. Rev. B* **2000**, *62*, 10958; b) T. Tsuzuki, S. Tokito, *Adv. Mater.* **2007**, *19*, 276.

[15] a) G. Lin, H. Peng, L. Chen, H. Nie, W. Luo, Y. Li, S. Chen, R. Hu, A. Qin, Z. Zhao, B. Z. Tang, *ACS Appl. Mater. Interfaces* **2016**, *8*, 16799; b) J. Y. Kim, T. Yasuda, Y. S. Yang, C. Adachi, *Adv. Mater.* **2013**, *25*, 2666; c) H. Nie, B. Chen, J. Zeng, Y. Xiong, Z. Zhao, B. Z. Tang, *J. Mater. Chem. C* **2018**, *6*, 3690.

[16] J. Chen, J. Zeng, X. Zhu, J. Guo, Z. Zhao, B. Z. Tang, *CCS Chemistry* **2021**, *3*, 230.

[17] H. Uoyama, K. Goushi, K. Shizu, H. Nomura, C. Adachi, *Nature* **2012**, *492*, 234.

[18] Q. Zhang, H. Kuwabara, W. J. Potscavage Jr., S. Huang, Y. Hatae, T. Shibata, C. Adachi, *J. Am. Chem. Soc.* **2014**, *136*, 18070.

[19] a) D. Ding, Z. Wang, C. Li, J. Zhang, C. Duan, Y. Wei, H. Xu, *Adv. Mater.* **2020**, *32*, 1906950; b) W. Li, B. Li, X. Cai, L. Gan, Z. Xu, W. Li, K. Liu, D. Chen, S.-J. Su, *Angew. Chem., Int. Ed.* **2019**, *58*, 11301; c) J. Zhang, C. Han, F. Du, C. Duan, Y. Wei, H. Xu, *Adv. Funct. Mater.* **2020**, *30*, 2005165; d) P. Wei, D. Zhang, L. Duan, *Adv. Funct. Mater.* **2019**, *30*, 1907083.